Purdue University
Purdue e-Pubs

CTRC Research Publications | Cooling Technologies Research Center

3-1-2023

Intra-lid multi-core vapor chamber architecture for heterogeneous electronic packages: technology concept to prototype evaluation

S Bandyopadhyay

A Yuksel

A M. Marconnet

Justin Weibel
jaweibel@purdue.edu

Follow this and additional works at: https://docs.lib.purdue.edu/coolingpubs

Bandyopadhyay, S; Yuksel, A; Marconnet, A M.; and Weibel, Justin, "Intra-lid multi-core vapor chamber architecture for heterogeneous electronic packages: technology concept to prototype evaluation" (2023). *CTRC Research Publications.* Paper 399.
http://dx.doi.org/https://doi.org/10.1109/TCPMT.2022.3230044

This document has been made available through Purdue e-Pubs, a service of the Purdue University Libraries. Please contact epubs@purdue.edu for additional information.

Intra-lid Multi-Core Vapor Chamber Architecture for Heterogeneous Electronic Packages: Technology Concept to Prototype Evaluation

Soumya Bandyopadhyay[1], Anil Yuksel[2], Amy M. Marconnet[1], Justin A. Weibel[1]

***Abstract* — Thermal management of future heterogeneous electronic packages with extreme heat fluxes relies on effective spreading of heat in the package lid. Intra-lid integration of vapor chambers is a promising strategy for simultaneous dissipation of large total heat loads and localized high-flux hotspots. However, conventional vapor chambers comprising a single vapor core require relatively thick evaporator wicks to prevent dry out at high total heat loads, thereby imposing a large temperature drop across the wick at the hotspot location. We recently proposed a cascaded multi-core vapor chamber (CMVC) architecture comprising a single-core vapor chamber stacked on an array of smaller footprint vapor cores having relatively thinner wicks. The multi-core array is designed to spread heat from arbitrarily distributed high-flux hotspots before they enter the top vapor chamber having a thicker wick. Then, the top vapor chamber spreads the high total heat loads to the base of the mounted heat sink. To evaluate the proposed CMVC technology, we make a weighted decision to identify an appropriate minimum viable prototype for subsequent design and testing. A reduced-order model is used to determine the dimensions and properties of the wick and vapor core that minimize the temperature drop across the down-selected multi-core vapor chamber architecture for a given power map, considering manufacturing process constraints. Finite element analysis (FEA) simulations are employed to decide a condenser wall thickness that avoids permanent deformation in the vapor chamber architecture under a mechanical load. A prototype is manufactured by a commercial vendor following these parameters and manufacturing constraints. As predicted by the thermal model, experimental characterization of this first-reported multi-core vapor chamber array prototype offers a notable reduction in temperature drop relative to a benchmark solid copper spreader, owing to attenuation of hotspots at a low temperature difference.**

Keywords— heterogeneous integration, electronics packaging, vapor chamber, hotspot, non-uniform

Nomenclature

Q	heat input
q''	heat flux
T	temperature
x	length

Subscripts

bg	background
cp	cold plate
evap	evaporator
hs	hotspot
sp	spreader

[1]The authors are with the School of Mechanical Engineering, Purdue University, West Lafayette, IN 47907 USA. (e-mails: bandyop0@purdue.edu; amarconn@purdue.edu; jaweibel@purdue.edu).[2]The author is with IBM Systems, IBM Corporation, Austin, TX 78758 (e-mail: Anil.Yuksel@ibm.com)

I. INTRODUCTION

The current revolution in semiconductor electronics involves the heterogeneous integration of many different chiplet-based designs within the same package to enable functionality greater than the sum of its parts. The heterogeneity in functional components, coupled with their time-dependent workloads, leads to spatiotemporally non-uniform package-internal heat generation that requires manufacturable and scalable thermal solutions within the constraints of the device envelope. In particular, such solutions must address spatial non-uniform power maps comprising a large total heat load from the low heat flux background interspersed simultaneously with high-density hotspots. In typical electronic packages, the package lid must effectively spread these high local heat fluxes, ultimately dissipating the total heat load using a mounted heat sink [1]. The presence of interfaces between these multiple stacked components impedes the flow of heat, causing excessive temperature rise and thereby affecting the device reliability. In this context, embedding improved performance heat spreaders into the package lid can be a strategy to lower excessive temperatures by allowing lateral diffusion from arbitrarily located hotspots within the package.

Vapor chambers have been established as reliable passive thermal management solutions for electronic devices [2]. Vapor chambers comprise a sealed chamber lined on the inside walls by porous wicks that act as a capillary pump to passively circulate an internal working fluid. The working liquid evaporates at the heat source where the latent heat is absorbed. The generated vapor spreads throughout the inner core, condenses over a larger area, and rejects heat to be subsequently dissipated to a heat sink or cold plate. The condensed liquid is continuously drawn back to the location of heat input by capillary action in the wick, where the cycle repeats. The reliable and passive operation of vapor chambers casts them as strong candidates for scalable integration into high-power heterogeneous package lids.

Extensive research has focused on design of the evaporator wick structures inside of a vapor chamber to address the removal of high heat fluxes over differing heat input areas [3]. Mono-porous sintered metal powders and screen wicks offer high capillary pumping forces as well as high effective thermal conductivities [4]. This has motivated detailed experimental investigation of the effect of their porous geometry and thickness on heat transfer performance in copper screens [5,6] and sintered powders [8] under capillary-fed evaporation and boiling. Other studies [7] have experimentally studied the effect of the amount of liquid charge on the relative difference in performance of vapor chambers having different wick types.

Further investigations have aimed to engineer the macroscale patterning of wicks to dissipate high total power over relatively large evaporator areas at uniform heat fluxes. These include: hierarchical wick structures [9, 10, 11] having two characteristic pore sizes for simultaneously improving permeability and enhancing capillary limit; two-layer evaporator wicks [12,13] designed to replenish liquid over a large area; and grid-patterned wick structures [14] for extracting vapor arising from boiling in wick structures. On the contrary, several studies have focused on development of novel wick microstructures targeted towards dissipating extreme heat fluxes from smaller hotspot areas while maintaining low surface superheat. These include copper inverse opal wicks [15] and carbon nanotube bi-porous wick structures [16,17], to name a couple.

Alternatively, at the component-scale, several studies have explored the design and characterization of novel vapor chamber architectures that modify the internal layout and wick structure to improve performance [18] by affecting bulk fluid recirculation. Koukoravas et al. [19] performed an experimental characterization of a vapor chamber having a condenser with patterned wettability. Hwang et al. [20] built and experimentally characterized a vapor chamber architecture wherein the evaporator and condenser wicks are interconnected by multiple wick columns to facilitate liquid resupply. Chen et al. [21] performed experiments with vapor chambers comprising multi-artery reentrant microchannels, distributed radially, under a uniform heat flux. Various additional studies have experimentally investigated the performance of vapor chambers, but always subject to uniform heat fluxes such as supplied by serpentine heaters [22] or generated by cartridge heaters inserted inside a copper heater block [23].

Studies in the literature that have focused either design of the evaporator wick or alterations in the vapor chamber internal architectures have not been developed for (or characterized under) conditions where there exists both low heat flux background power and high heat flux hotspots, despite the importance and prevalence of such heterogenous power maps. To address this gap, our recent work introduced [24], performed a model-based parametric optimization [25], and experimentally demonstrated the rationale behind [26] a cascaded multi-core vapor chamber (CMVC) designed to spread a total background heat load from the entire die area, while also minimizing the temperature rise associated with high heat flux hotspots. The CMVC architecture has a bottom-tier multi-core vapor chamber comprising an array of many tiny vapor cores covering the die footprint. Each individual core attenuates high heat flux hotspots at a low temperature difference before the heat passes through to a single large vapor core that functions as a conventional vapor chamber in the top tier.

Although promising in theory, multi-core vapor chambers have not been previously fabricated or characterized. The present study aims to evaluate the functionality of a multi-core vapor chamber architecture for dissipating heat from non-uniform power maps, by demonstrating that a multi-core vapor chamber prototype offers lower temperature drop relative to a benchmark copper spreader. First, based on the proposed cascaded multi-core vapor chamber technology, we identify a minimum viable prototype that will demonstrate the novel functional characteristics of the CMVC. Next, the prototype design, manufacturing, and testing methodologies are introduced. In the results, the performance of the heat spreaders is compared by reporting the trends in measured temperatures as a function of the hotspot and background heat fluxes applied from a non-uniform power map.

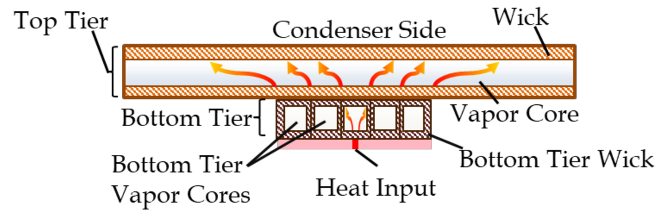

Fig. 1. Schematic cross-sectional drawing (not to scale) of the cascaded multi-core vapor chamber (adapted from [25]) with inset magnified view of the bottom tier having an array of small vapor cores, over multiple hotspots (dark red) and background heat input (pink bar) over the entire width.

II. Evaluation of Proposed Technology

A. Identification of a Minimum Viable Prototype

The proposed cascaded multi-core vapor chamber technology, as depicted in Figure 1 [25], has two distinct tiers - a top tier having a single vapor core and a bottom tier having an array of many smaller vapor chambers/cores. The top tier is functionally identical to a conventional single-layer vapor chamber, the efficacy and functionality of which is well understood and has been demonstrated in literature and products. In the bottom tier vapor chamber array, each individual vapor core is designed to attenuate a small hotspot, before it enters the top tier, using a very thin wick structure that imposes a small conduction resistance. To determine a minimum viable prototype to demonstrate the technology, we considered several different possible prototype constructions. The primary candidates were a complete cascaded multi-core vapor chamber with a bottom and top tier versus a standalone bottom tier multi-core vapor chamber array comprising a square array of individual cores. A weighted decision was taken that the bottom tier of the cascaded multi-core vapor chamber is the best candidate for a minimum viable prototype. This architecture can demonstrate the key functionality of individual cores for hotspot dissipation and assess the manufacturing feasibility of a multi-core array, without the added complexity and manufacturing cost of interfacing with a conventional vapor chamber for which the thermal behavior is already well known.

B. Summary of Prototype Design Process

The vapor chamber prototype, representative of the bottom-tier multi-core architecture, was designed to minimize temperature drop while ensuring that it can withstand the mechanical load applied during testing. In particular, any significant deformation of the vapor chamber walls, even if not causing mechanical damage, would reduce the vapor core thicknesses and increase the temperature drop inside the vapor core.

The following subsection report the design, fabrication, and testing of the vapor chamber prototype having an evaporator footprint of 25 mm × 25 mm with a maximum

through-plane thickness of 1 mm. These dimensions are based on the footprint area of the target power map and overall lid thickness constraints. The power map employed for our in-house testing of the prototype has a maximum hotspot heat flux of 125.5 W/cm^2 over 5 mm × 5 mm and a background heat flux of 6.7 W/cm^2 over the remaining area in the 25 mm × 25 mm footprint. We have designed for a case where the hotspot lies at the intersection underneath four cores in the array. This effectively means that each of these four individual vapor cores is subjected to the hotspot heat flux over 2.5 mm × 2.5 mm, at the corner of the vapor core, and an additional background flux over remainder of the core. A model, previously developed and described in detail in [25], was employed to minimize the total temperature drop within the wicks and the vapor core of the bottom tier. The model yields the corresponding wick properties (namely, thickness, porosity, and particle diameter) and the vapor core geometry (namely, footprint area and thickness). The thickness of the copper evaporator wall was chosen to be the minimum allowable thickness by the manufacturing methods, 0.2 mm, as this minimized the temperature drop due to conduction in the evaporator wall. Once the dimensions of the wick, vapor core, and evaporator wall are obtained, a static stress analysis is conducted using finite element analysis (FEA) simulations to obtain the minimum wall thickness of the condenser copper wall that ensuring there is no plastic deformation of the vapor chamber prototype. For the static stress analysis, the maximum Von-Mises stress was computed at different points of the vapor chamber prototype and compared against the yield stress of copper. Results obtained from the models, and the corresponding design parameters for the prototype, are reported below in Sections III.A and III.B of this paper.

III. Design of Experiments

A test facility is used to characterize the temperature drop across a solid copper spreader and the multi-core vapor chamber prototype subject to the same non-uniform heat input while dissipating heat to a cold plate, as shown in Figure 2(a). The copper spreader (see Figure 2(c)) has the same outer dimensions of 25 mm × 25 mm × 1 mm as the vapor chamber prototype (see Figure 2(d)). The non-uniform power map (see the plan view in Figure 2(b)) has a hotspot heat load (Q_{hs}) over the center 25 mm^2 (denoted by red). This centrally located hotspot is surrounded by a background heat flux (denoted by pink) over an area having an edge length (x_{bg}) of 25 mm that generates a uniform total background power (Q_{bg}).

A. Testing facility

A test facility with the components shown in Figure 3 is used for evaluating the maximum temperature difference of heat spreaders at differing heat loads, with modifications to the heating configuration as compared to the facility previously reported in [26]. Heat spreaders can be attached to the top surface of a 5 mm × 5 mm × 30 oxygen-free copper block, heated by a cartridge heater (35025K111, McMaster-Carr) inserted into the bottom 10 mm × 10 mm × 30 mm section. The copper block is thermally insulated within polyether ether ketone (PEEK) walls. A custom-designed polyimide film heater (Tramonto Circuits) having a 25 mm × 25 mm footprint, with a 5 mm × 5 mm cut-out in the center, is attached to the bottom of the heat spreaders, surrounding the central copper heater block, using pressure-sensitive adhesive. The bottom of the copper block rests on an insulating ceramic base and mineral wool insulation is loosely packed in the void space between the copper block, ceramic, and the surrounding PEEK walls. The copper block has a rake of four thermocouples positioned along the centerline. The surrounding insulation ensures one-dimensional heat flow in the block, enabling measurement of the heat flux based on the temperature gradient and the surface temperature by extrapolation. The top surface of the copper block protrudes slightly (~1 mm) out of the surrounding top PEEK for ease of attaching the heat spreaders.

B. Testing procedure

Tests are performed with the copper spreader and the multi-core vapor chamber prototype for different hotspot heat fluxes at a given background heat flux. To compare the performance of copper and vapor chamber prototype under equal conditions, the liquid temperature in the refrigerating bath circulator is maintained at a constant temperature. The hotspot heat flux (q''_{hs}) applied through the copper block is incremented from 11.5 W/cm^2 to 125.5 W/cm^2. At every hotspot heat flux level, the background heat flux (q''_{bg}) applied using the film heater is maintained at 6.7 W/cm^2. The tests are designed to ensure that there is a significant contrast between the hotspot and the background (a factor of ~2 to 20) when comparing the performance of the prototype to copper. During the tests, the hotspot and background heat fluxes are controlled using separate power sources. For each combination of hotspot and background heat flux, steady-state data are recorded for the respective heat spreaders once the system temperatures become constant (a change less than ~0.01 °C/s), which takes ~30 min between successive hotspot heat fluxes.

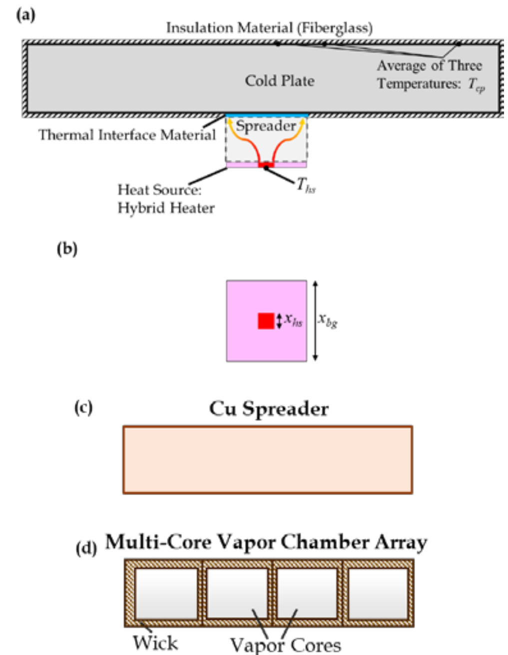

Fig. 2 (a) Schematic cross-section of the heat spreader boundary conditions in the experiment. (b) Top view of the representative power map footprint comprising a hotspot (red) heat load of side length x_{hs}, centered on the background (pink) heat flux of side length x_{bg}. Schematic cross-sections of the (c) solid copper and (d) multi-core vapor chamber prototype.

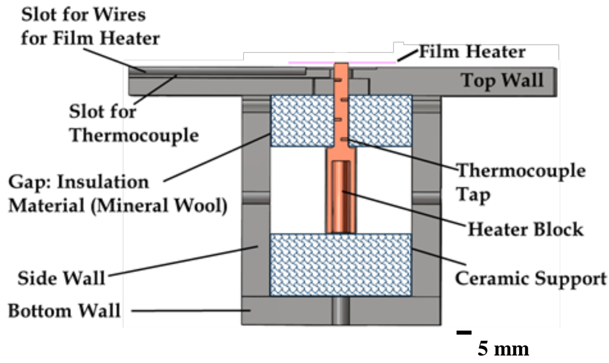

Fig. 3 Sectional cut view of the heater block testbed for experimental characterization of a heat spreader. A copper heater block insulated by ceramic and PEEK provides a uniform heat flux to the base of the heat spreader soldered atop. Thermocouples (not shown) are used to measure the temperature gradient along the centerline of the copper block for estimating the heat input to the spreader. The film heater (pink; separately shown for clarity) is fixed at the base of the heat spreader surrounding the heater block.

C. Data reduction

All thermocouples used for temperature measurement are ice-point-referenced (TRCIII, Omega) and calibrated using a dry-block calibrator (Jupiter 4852 Advanced, Isotech). The temperature gradient, measured from a linear fit to a rake of four thermocouples inside the copper heater block, is employed to estimate the hotspot heat flux to a given heat spreader. Uncertainty in the measured hotspot heat flux is estimated to be less than 4% based on the calibrated uncertainties in the temperature (± 0.2 °C) and the location of the measurements. The maximum temperature at the top surface (T_{hs}) of the heater block is measured by linear extrapolation of the temperatures measured by the rake of four thermocouples inside the heater block. The uncertainties related to the hotspot heat load from the heater block are calculated as described in [27]. The liquid temperature in the refrigerating bath circulator (T_{bath}) has a documented uncertainty of ± 0.05 °C. The voltage across the film heater is measured using a data acquisition system and the background heat flux is subsequently calculated using the electrical resistance of the film heater. The uncertainty in the background heat load is estimated from the uncertainties in the measured voltage and the electrical resistance of the film heater. Heat losses from the film heater are within the uncertainty bounds reported in the results.

The primary performance metric considered for both the copper and the vapor chamber prototype is the maximum temperature rise of the hotspot above the constant temperature bath, calculated as:

$$\Delta T_{hs,bath} = T_{hs} - T_{bath} \quad . \tag{1}$$

This temperature difference includes the temperature difference inside the heat spreader technology and the temperature drop in external components that are maintained constant. We were particularly careful to ensure that the total temperature drop across the heater block-spreader interface and the spreader-cold plate interface were consistent between tests by first performing multiple tests with the copper spreader under the same conditions (reported below in the Section III.C). This ensures that the comparison of heater spreads based on this measured maximum temperature rise of the hotspot is only a signature of the relative performance difference between the copper and vapor chamber prototype.

IV. Results

Static FEA simulations are first employed to predict the minimum thickness of the wall of the condenser required to keep the minimum factor of safety of design above a desired threshold. Next, the thermal model is employed to predict the expected relative improvement in performance of the multi-core vapor chamber prototype relative to the solid copper benchmark. Details of the manufacturing process and the dimensions of the important features of the prototype are then discussed. Finally, the results of experimental tests with the solid copper benchmark and the vapor chamber prototype are then compared at different hotspot heat fluxes for a given background flux.

A. Predictions from Models

A parametric thermal performance design optimization [25] of the cascaded multi-core vapor chamber architecture indicates that a sintered wick should have properties in the range of 50-60% porosity, 15 – 20 µm particle diameter, and 60 – 80 µm wick thickness. Further, the manufacturing process of the prototype (discussed in Section III.B below) allows a minimum evaporator wall thickness of 0.2 mm. A total load of 7.5 kg (73.5 N) is applied on the condenser wall of the vapor chamber prototype during testing. Static FEA simulations are performed to ensure that the condenser wall can support the external load.

The FEA simulations are performed in SolidWorks Static Structural software and follow standard analysis techniques to solve the three-dimensional state of stress equations. The boundary conditions and simulation domain, as illustrated Figure 4a, evenly distribute the total load over the top of the condenser wall. The condenser wall is supported above the evaporator wall, which is fixed from below, by the surrounding walls. Each core is centrally supported by a 2 mm diameter pillar (treated as rigid support) that connects between the evaporator and the condenser wall. The internal wick structures forming the walls of the individual vapor cores inside the multi-core prototype would likely provide additional support of the condenser wall. However, their presence is neglected as a conservative assumption in the FEA simulations. The domain is meshed with tetrahedral elements; the solution is confirmed to achieve grid-independence when using elements with an edge length of ~0.6 mm (~40 grid points across the face of the condenser on which the load is acting).

From the static mechanical FEA simulations, the resulting maximum Von-Mises stress is predicted as a function of condenser wall thickness. Figure 4b shows the variation of this Von-Mises stress across the top surface of the condenser, the plane where the stress is maximum, when the thickness of the condenser wall is 100 µm. Figure 4c plots the factor of safety (ratio of the maximum Von-Mises stress at the top surface of the condenser and the yield stress) against the thickness of the condenser wall. Given a target factor of safety of 3, as indicated by the dashed horizontal line, a minimum condenser wall thickness of 0.1 mm is required.

Thermal model predictions consider these dimensions and the properties of the wick, vapor core, and evaporator wall,

thermal. The bar chart in Figure 4d compares the temperature drop of the optimized multi-core vapor chamber architecture to the solid copper (Cu) benchmark, for the maximum hotspot heat flux of 125.5 W/cm^2 and a background flux of 6.7 W/cm^2. The temperature rise across the spreader is larger for the solid copper benchmark (17.1 ℃) compared to the optimized multi-core vapor chamber (1.6 ℃). In the manufactured prototypes, the presence of cylindrical pillars in the cores would increase the temperature drop inside the multi-core architecture, but results from models still indicates a significant margin of improvement is available.

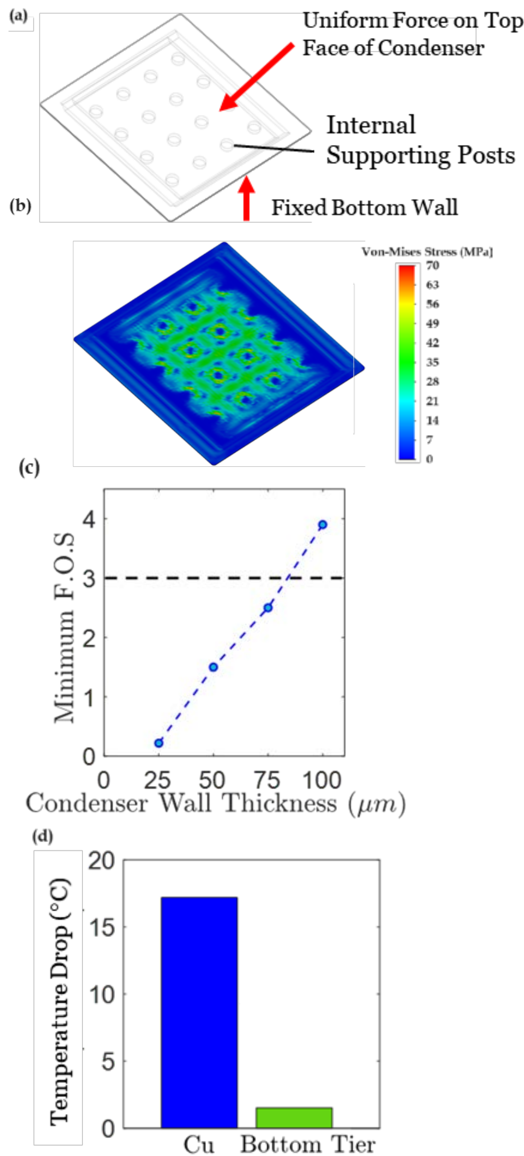

Fig. 4 (a) Multi-core vapor chamber prototype geometry used for mechanical FEA simulations, indicating the condenser wall on which there acts distributed force; for scale, the outer dimension is 25 mm × 25 mm. (b) Von-Mises stress across the top surface of the condenser of the vapor chamber prototype geometry. (c) Variation of the predicted factor of safety with the thickness of the condenser wall. (d) Model-based comparison of the maximum temperature rise across the solid copper benchmark (Cu) and the multi-core vapor chamber prototype for a hotspot heat flux of 125.5 W/cm^2 and a background flux of 6.7 W/cm^2.

B. Manufactured Prototype

The multi-core vapor chamber prototype was manufactured by Delta Inc. The manufactured prototype (see Figure 5) has 16 discrete vapor cores separated by 1 ± 0.1 mm thick porous wick structures. The evaporator wick is a thin copper mesh having a thickness of 60 µm. The prototype has a square cross-section of edge length 25 ± 0.1 mm having an outer wall thickness of 0.2 ± 0.02 mm. Each small vapor core is connected by gas paths to a single filling location to ensure each small cavity can be quickly and effectively evacuated during the vapor chamber charging process. The filling pipe embedded inside the vapor chamber sidewall has a press-fit depth of 50 µm that allows sealing off of the pipe after the charging process without adding any height to the overall device. To accommodate the sealing, the condenser of the prototype has a 3 mm rim of excess width relative to the evaporator wall and is manufactured to have a thickness of 0.1 ± 0.01 mm. In order to ensure that the mechanical stresses induced by the weight applied to the vapor chamber do not cause permanent deformation, each core is structurally supported at the center by a 2 ± 0.2 mm diameter bracing column made from 80 – 120 µm sintered copper particles. These porous bracing columns also adds another path of liquid return to the evaporator wick that would increase the capillary limit of the prototype vapor chamber.

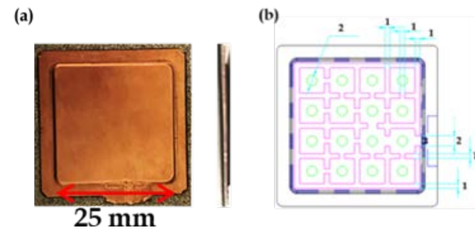

Fig. 5 (a) Picture of the manufactured vapor chamber prototype showing the evaporator-side face (left) and a side view (right). (b) Schematic sectional view of the multi-core vapor chamber prototype with different features. Pink lines denote the wick structures separating each vapor core. Green circles denote bracing columns. All dimensions are in mm.

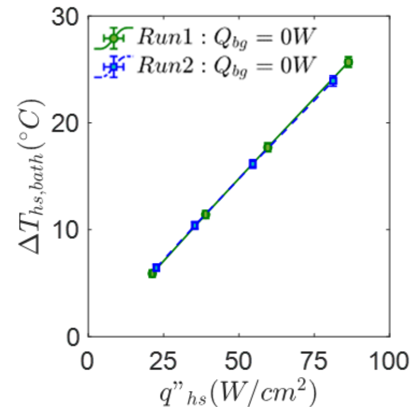

Fig. 6 Hotspot temperature rise as a function of the hotspot heat flux, comparing two repeated test runs for the solid copper heat spreader, without any background heat load.

C. Experimental Measurements: Repeatability

Repeatability testing was performed to ensure that the experimental apparatus provided consistent results from test-to-test. Multiple test runs were performed with solid copper heat spreaders; between each test run, the apparatus was disassembled and reassembled to freshly insert the sample between the heater block and cold plate. This procedure ensures consistency of the assembly processes and interface resistances in the experimental facility, such that the measured overall temperature rise of the hotspot is only a signature of the relative performance difference between the copper and multi-core vapor chamber prototype. For these tests, the liquid temperature in the refrigerating bath circulator is maintained at 50 °C.

The temperature rise at the hotspot for the solid copper spreader is shown as a function of the hotspot heat flux in Figure 6 for two repeated test runs. The maximum temperature drop linearly increases as the hotspot heat flux is increased for each given run, as expected for a constant temperature drop associated with conduction through the heat spreader and other elements of the test facility. Most importantly the variability in the maximum hotspot temperature rise of the copper spreader between both repeated test runs is less than the measurement uncertainty. This result confirms that the temperature differences across the components external to the heat spreader in the test assembly are same between multiple sets of tests.

D. Experimental Measurements: Copper vs. Multi-Core Vapor Chamber Prototype

The measured hotspot temperature rise of the multi-core vapor chamber prototype is compared to the solid copper benchmark as a function of hotspot heat fluxes in Figure 7. For these tests, the liquid temperature in the refrigerating bath circulator is maintained at 60 °C, and the background flux is kept fixed at 6.7 W/cm^2. Tests with the copper spreader are conducted up to a hotspot flux of 49.7 W/cm^2. Above this value of the hotspot heat flux, only for the copper heat spreader, a non-uniformity in the measured cold plate temperature occurs as the copper is unable to effectively spread the high hotspot heat fluxes, compromising the uniform boundary condition that must be held in place for a direct comparison. Hence, the temperature rise for the solid copper is linearly extrapolated (as shown by the dashed portion of the line) as such a heat-load-independent conduction thermal resistance is well-established and also shown in our data at lower heat fluxes. This extrapolation is not needed for the vapor chamber prototype (dash-dotted line), for which all data shown are direct measurements.

For this tested background heat flux, the hotspot temperature rise monotonically increases as the hotspot heat flux is increased for both spreaders as expected. However, the vapor chamber prototype offers a notable reduction in the hotspot temperature of ~4 °C relative to the solid copper spreader for every hotspot heat flux. For example, when the hotspot heat flux is ~55 W/cm^2, the maximum temperature drop of the multi-core vapor chamber prototype of ~28.8 °C was ~13% lower than the benchmark copper spreader temperature drop of ~33.2 °C. Considering that the hotspot temperature rise here includes all of the additional interfacial resistances in the test facility between the hotspot and the coolant, this result indicates a significant reduction in temperature drop across the heat spreading layer, consistent with the model predictions. This confirms the ability of the individual vapor cores to attenuate the high hotspot heat flux while simultaneously subjected to the background power, at a temperature difference much lower than solid copper. This promising result confirms the viability of a multi-core vapor chamber architecture, and thereby the CMVC concept, as a strategy for effective intra-lid heat spreading from non-uniform power maps having combined hotspots and a background heat input.

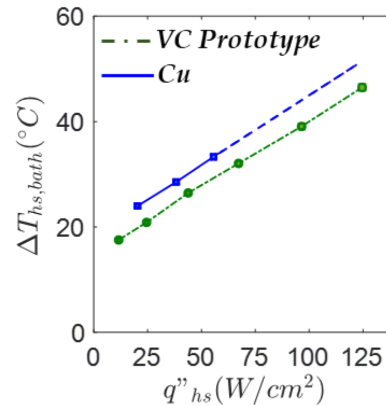

Fig. 7 Hotspot temperature rise as a function of the hotspot heat flux (at a constant background heat flux of 6.7 W/cm^2), comparing the solid copper benchmark (Cu; solid line and extrapolated dashed line) and multi-core vapor chamber prototype (VC; dash-dotted line).

V. Conclusion

Intra-lid cascaded multi-core vapor chambers (CMVC) hold promise for simultaneously dissipating high total powers and intense local heat fluxes at a low temperature drop, for thermal packaging of heterogeneously integrated electronic components. The viability of this CMVC technology rests on the ability of a bottom-tier multi-core vapor chamber array to locally diffuse hotspots, which had not been previously demonstrated. This work fabricates and tests a multi-core vapor chamber prototype, guided by a reduced-order thermal model and mechanical finite element analysis simulations to select the wick properties and vapor core dimensions. The multi-core vapor chamber architecture was designed to minimize the temperature rise of hotspots and ensure the mechanical integrity of a prototype. These design parameters, coupled with practical manufacturing constraints and considerations, were subsequently used to guide the manufacture of the prototype by a commercial vendor. Experimental testing demonstrates successful performance of the multi-core vapor chamber prototype, which offers notable reduction in the hotspot temperature under a non-uniform heat load, relative to a solid copper spreader. In particular, for the given range of testing parameters and background heat flux, the prototype offers a maximum reduction in the hotspot temperature rise by ~4 °C. Considering the entire testing assembly, this reduction is commensurate with the model predictions, and confirms the viability of the multi-core vapor chamber architecture.

ACKNOWLEDGMENT

This work was supported by Semiconductor Research Corporation (SRC), as a part of the Global Research Collaboration (GRC) Program on Packaging (PKG; Science Director, Dr. John Oakley) in the Center for Heterogeneous Integration Research on Packaging (CHIRP). We are thankful to the SRC liaisons, Dr. Rajiv Mongia, Dr. Feras Eid, Dr. Kamal Sikka for their discussion and input on the work.

REFERENCES

[1] IEEE Heterogeneous Integration Roadmap: Chapter 3 (https://eps.ieee.org/images/files/HIR_2020/ch03_iot.pdf)

[2] Bulut, M., Kandlikar, S.G., and Sozbir, N., 2019. A review of vapor chambers. *Heat Transfer Engineering*, **40**(19), pp.1551-1573.

[3] Weibel, J.A. and Garimella, S.V., 2013. Recent advances in vapor chamber transport characterization for high-heat-flux applications. *Advances in Heat Transfer*, **45**, pp. 209-301.

[4] Faghri, A., 1995. *Heat Pipe Science and Technology*. Taylor & Francis, Washington, DC.

[5] Li, C., Peterson, G. P., and Wang, Y., 2006, Evaporation/Boiling in thin capillary wicks (l) – wick thickness effects, *Journal of Heat Transfer*, **128**(12), pp. 1312–1319.

[6] Li, C., Peterson, G. P., and Wang, Y., 2006, Evaporation/Boiling in thin capillary wicks (II) – effects of volumetric porosity and mesh size, *Journal of Heat Transfer*, **128**(12), pp. 1312–1319.

[7] Chen, L., Deng, D., Huang, Q., Xu, X. and Xie, Y., 2020. Development and thermal performance of a vapor chamber with multi-artery reentrant microchannels for high-power LED. *Applied Thermal Engineering*, **166**, p.114686.

[8] Weibel, J.A., Garimella, S.V. and North, M.T., 2010. Characterization of evaporation and boiling from sintered powder wicks fed by capillary action. *International Journal of Heat and Mass Transfer*, **53**(19-20), pp.4204-4215.

[9] Ju, Y.S., Kaviany, M., Nam, Y., Sharratt, S., Hwang, G.S., Catton, I., Fleming, E., and Dussinger, P., 2013. Planar vapor chamber with hybrid evaporator wicks for the thermal management of high-heat-flux and high-power optoelectronic devices. *International Journal of Heat and Mass Transfer*, **60,** pp.163-169.

[10] Hwang, G.S., Nam, Y., Fleming, E., Dussinger, P., Ju, Y.S., and Kaviany, M., 2010. Multi-artery heat pipe spreader: experiment. *International Journal of Heat and Mass Transfer*, **53**(13-14), pp.2662-2669.

[11] Semenic, T. and Catton, I., 2009. Experimental study of biporous wicks for high heat flux applications. *International Journal of Heat and Mass Transfer*, **52**(21-22), pp.5113-5121.

[12] Sudhakar, S., Weibel, J.A., Zhou, F., Dede, E.M., and Garimella, S.V., 2019. Area-scalable high-heat-flux dissipation at low thermal resistance using a capillary-fed two-layer evaporator wick. *International Journal of Heat and Mass Transfer*, **135**, pp.1346-1356.

[13] Sudhakar, S., Weibel, J.A., Zhou, F., Dede, E.M., and Garimella, S.V., 2020. The role of vapor venting and liquid feeding on the dryout limit of two-layer evaporator wicks. *International Journal of Heat and Mass Transfer*, **148**, p.119063.

[14] Weibel, J.A. and Garimella, S.V., 2012. Visualization of vapor formation regimes during capillary-fed boiling in sintered-powder heat pipe wicks. *International Journal of Heat and Mass Transfer*, **55**(13-14), pp.3498-3510.

[15] Palko, J.W., Zhang, C., Wilbur, J.D., Dusseault, T.J., Asheghi, M., Goodson, K.E., and Santiago, J.G., 2015. Approaching the limits of two-phase boiling heat transfer: High heat flux and low superheat. *Applied Physics Letters*, **107**(25), p.253903.

[16] Cai, Q. and Bhunia, A., 2012. High heat flux phase change on porous carbon nanotube structures. *International Journal of Heat and Mass Transfer*, **55**(21-22), pp.5544-5551.

[17] Cai, Q. and Chen, Y.C., 2012. Investigations of biporous wick structure dryout. *Journal of Heat Transfer*, **134**(2), p.021503.

[18] Weibel, J.A. and Garimella, S.V., 2013. Recent advances in vapor chamber transport characterization for high-heat-flux applications. *Advances in Heat Transfer*, **45**, pp. 209-301.

[19] Koukoravas, T.P., Damoulakis, G., and Megaridis, C.M., 2020. Experimental investigation of a vapor chamber featuring wettability-patterned surfaces. *Applied Thermal Engineering*, **178**, p.115522.

[20] Hwang, G.S., Nam, Y., Fleming, E., Dussinger, P., Ju, Y.S., and Kaviany, M., 2010. Multi-artery heat pipe spreader: experiment. *International Journal of Heat and Mass Transfer*, **53**(13-14), pp.2662-2669.

[21] Chen, L., Deng, D., Huang, Q., Xu, X. and Xie, Y., 2020. Development and thermal performance of a vapor chamber with multi-artery reentrant microchannels for high-power LED. *Applied Thermal Engineering*, **166**, p.114686.

[22] Liu, T., Dunham, M.T., Jung, K.W., Chen, B., Asheghi, M., and Goodson, K.E., 2020. Characterization and thermal modeling of a miniature silicon vapor chamber for die-level heat redistribution. *International Journal of Heat and Mass Transfer*, **152**, p.119569.

[23] Wang, M., Cui, W., and Hou, Y., 2019. Thermal spreading resistance of grooved vapor chamber heat spreader. *Applied Thermal Engineering*, **153**, pp.361-368.

[24] Bandyopadhyay, S., Marconnet, A.M. and Weibel, J.A., 2020. A Cascaded Multi-Core Vapor Chamber for Intra-Lid Heat Spreading in Heterogeneous Packages. *19th IEEE Intersociety Conference on Thermal and Thermomechanical Phenomena in Electronic Systems (ITherm)*, pp. 963-969.

[25] Bandyopadhyay, S., Marconnet, A.M. and Weibel, J.A., 2021. Cascaded Multicore Vapor Chambers for Intrapackage Spreading of High-Power, Heterogeneous Heat Loads. *IEEE Transactions on Components, Packaging and Manufacturing Technology*, ***11***(6), pp.944-954.

[26] Bandyopadhyay, S., Lohitnavy, N., Marconnet, A.M. and Weibel, J.A., 2021, June. Experimental Characterization of Cascaded Vapor Chambers for Spreading of Non-Uniform Heat Loads. In *2021 20th IEEE Intersociety Conference on Thermal and Thermomechanical Phenomena in Electronic Systems (iTherm)* (pp. 280-284). IEEE.

[27] Sarangi, S., Weibel, J.A., and Garimella, S.V., 2015. Effect of particle size on surface-coating enhancement of pool boiling heat transfer. *International Journal of Heat and Mass Transfer*, **81**, pp.103-113.